Dielectric anisotropy in the *GW* space-time method

Christoph Freysoldt [a,1], Philipp Eggert [a], Patrick Rinke [a], Arno Schindlmayr [a,b], R.W. Godby [c], and Matthias Scheffler [a]

[a] *Fritz-Haber-Institut der Max-Planck-Gesellschaft, Faradayweg 4–6, 14195 Berlin, Germany*

[b] *Institut für Festkörperforschung, Forschungszentrum Jülich, 52425 Jülich, Germany*

[c] *Department of Physics, University of York, Heslington, York YO10 5DD, United Kingdom*

Abstract

Excited-state calculations, notably for quasiparticle band structures, are nowadays routinely performed within the *GW* approximation for the electronic self-energy. Nevertheless, certain numerical approximations and simplifications are still employed in practice to make the computations feasible. An important aspect for periodic systems is the proper treatment of the singularity of the screened Coulomb interaction in reciprocal space, which results from the slow $1/r$ decay in real space. This must be done without introducing artificial interactions between the quasiparticles and their periodic images in repeated cells, which occur when integrals of the screened Coulomb interaction are discretised in reciprocal space. An adequate treatment of both aspects is crucial for a numerically stable computation of the self-energy. In this article we build on existing schemes for isotropic screening and present an extension for anisotropic systems. We also show how the contributions to the dielectric function arising from the non-local part of the pseudopotentials can be computed efficiently. These improvements are crucial for obtaining a fast convergence with respect to the number of points used for the Brillouin zone integration and prove to be essential to make *GW* calculations for strongly anisotropic systems, such as slabs or multilayers, efficient.

Key words: *GW* approximation; anisotropic screening; Coulomb singularity; dielectric function
PACS: 71.15.Qe, 71.45.Gm

[1] email: freyso@fhi-berlin.mpg.de

1 Introduction

For describing quasiparticle excitations, as measured in direct and inverse photoemission, many-body perturbation theory in the GW approximation [1] has developed into the method of choice for weakly correlated solids and their surfaces. In particular, the GW approximation describes the quasiparticle band structures and band gaps for a large variety of semiconductors in good agreement with experimental results [2,3]. For more correlated systems, it becomes necessary to go beyond GW, but these schemes often include the GW self-energy diagrams as lowest order [4,5,6]. Similarly, the Bethe–Salpeter approach to electron-hole excitations, as probed in optical absorption or electron energy-loss spectroscopy, builds on the GW self-energy [7].

In the GW approximation the frequency-dependent, non-local self-energy Σ that connects the independent-particle Green function G_0 with the interacting one G is given by $\Sigma = \mathrm{i}GW$, where W is the dynamically screened Coulomb interaction. The independent-particle starting point is typically chosen to be the Green function of a Kohn–Sham density-functional theory (DFT) calculation. Despite significant methodological progress [8,9,10,11,12,13,14] GW calculations are still computationally demanding, and their application is limited to relatively small system sizes. So far all implementations employ a number of additional simplifications to reduce the computational cost. Some of these are motivated by physical considerations, such as plasmon-pole models [15] or model dielectric functions [16,17,18,19], while others appear as purely mathematical "tricks" to improve the numerical stability or efficiency. Often, the validity and usefulness of a specific approach depends on the physical system under consideration. An important aspect in every GW implementation that uses reciprocal space is the treatment of the singularity at $\mathbf{k} \to \mathbf{0}$ in the bare and screened interaction for non-metallic systems. This singularity is integrable, and many different schemes have been developed for these $\mathbf{k}$-space integrals [11,15,20,21,22,23]. The general idea is to describe the singular part by a model function that can be handled analytically, so that the remainder is sufficiently smooth for a numerical treatment. In physical terms, the $\mathbf{k} \to \mathbf{0}$ behaviour determines the long-range part of the interaction. The discretisation of the reciprocal-space integrals can then be interpreted as introducing an artificial supercell periodicity in real space. The periodic images of the quasiparticles give rise to an infinite self-interaction due to the $1/|\mathbf{r}|$ tail of the interaction. Any scheme that integrates the singularity analytically is therefore strictly equivalent to modifying the long-range behaviour of the interaction such that a quasiparticle does not interact with its periodic images or that the interaction decays faster than $1/|\mathbf{r}|^2$. In other words, different integration schemes correspond to particular modifications of the long-range tail and vice versa.

In most schemes screening is assumed to be isotropic at the length scale given by the inverse of the smallest non-zero **k**-vector, which is appropiate for most bulk materials but may fail in systems with an appreciable anisotropy, such as superlattices or layered materials, as well as in supercell approaches for low-dimensional materials like clusters, molecules, nanowires, films, or surfaces. An obvious way to avoid these spurious interactions for systems with broken translational symmetry is to abandon the concept of periodic boundary conditions altogether in the relevant directions and perform the calculation entirely in real space. For semi-infinite jellium surfaces such a GW embedding scheme has been successfully implemented [24,25]. Its extension to realistic surfaces, however, is computationally still too expensive. A real-space implementation for finite systems has also been reported [13,14], but its applicability to systems with periodicity in one or more directions remains to be shown.

Staying with the repeated-cell approach, we will show in the following how it is possible to incorporate the anisotropy in the treatment of the singularity in the GW space-time method [20]. In addition to the equations that we have implemented we derive exact expressions that allow us to discuss other algorithms in comparison. Furthermore, we will show that the proposed modifications considerably improve the convergence behaviour with respect to the number of **k**-points, which is the natural parameter associated with the singularity treatment. In practice the GW approximation is often applied non-self-consistently by constructing the screened interaction as well as the self-energy from the independent-particle Green function G_0. However, the behaviour of the anisotropy discussed in this article applies equally to the fully self-consistent GW approach. For simplicty we will therefore focus on the non-self-consistent case and indicate differences whenever they apply. In the interest of readability we will also refrain from introducing different symbols to distinguish between the self and non-self-consistent case.

This paper is organised as follows. In Section 2 we briefly describe the computation of the self-energy in the space-time method. In Section 3 we explain how the anisotropy is accounted for; the detailed derivation of the well-known anisotropic equations is presented in Appendix B for completeness. In Section 4 we demonstrate the improved **k**-point convergence behaviour resulting from our modifications before summarising our results in Section 5. In Appendix A we have collected the spherical-harmonics expansion of several vector quantities that appear in our derivations. Finally, an efficient implementation of the contribution from Kleinman–Bylander-type non-local pseudopotentials [26], which enter the expressions for the anisotropy, is presented in Appendix C. Unless otherwise indicated, we use Hartree atomic units.

2 Outline of the *GW* space-time method

The *GW* space-time method has been presented in detail elsewhere [20,27]. We will therefore only summarise the steps to construct the self-energy from the output of a preceding DFT calculation. Assuming a non-magnetic systems for simplicity (the extension to a spin-dependent Green function is straightforward), the computational steps are:

(1) Construction of the non-interacting Green function G in real space and imaginary time from the Kohn–Sham eigenfunctions $\varphi_{n\mathbf{k}}$ and eigenvalues $\epsilon_{n\mathbf{k}}$ (the Fermi level is set as the energy zero)

$$G(\mathbf{r},\mathbf{r}';\mathrm{i}\tau) = \mathrm{i}\frac{\Omega}{(2\pi)^3}\int_{\mathrm{BZ}}\mathrm{d}^3k \begin{cases} \sum\limits_n^{\mathrm{occ}} \varphi_{n\mathbf{k}}(\mathbf{r})\varphi^*_{n\mathbf{k}}(\mathbf{r}')\mathrm{e}^{-\epsilon_{n\mathbf{k}}\tau}, & \tau<0, \\ -\sum\limits_n^{\mathrm{unocc}} \varphi_{n\mathbf{k}}(\mathbf{r})\varphi^*_{n\mathbf{k}}(\mathbf{r}')\mathrm{e}^{-\epsilon_{n\mathbf{k}}\tau}, & \tau>0, \end{cases} \tag{1}$$

where Ω denotes the unit-cell volume and the integral over $\mathbf{k}$ runs over the first Brillouin zone,

(2) formation of the irreducible polarisability P in the random-phase approximation in real space and imaginary time

$$P(\mathbf{r},\mathbf{r}';\mathrm{i}\tau) = -2\mathrm{i}G(\mathbf{r},\mathbf{r}';\mathrm{i}\tau)G(\mathbf{r}',\mathbf{r};-\mathrm{i}\tau)\ , \tag{2}$$

(3) Fourier transformation of P to reciprocal space

$$P_{\mathbf{G}\mathbf{G}'}(\mathbf{k},\mathrm{i}\tau) = \frac{1}{\Omega}\int\mathrm{d}^3r\int\mathrm{d}^3r'\ P(\mathbf{r},\mathbf{r}';\mathrm{i}\tau)\mathrm{e}^{-\mathrm{i}(\mathbf{k}+\mathbf{G})\cdot\mathbf{r}+\mathrm{i}(\mathbf{k}+\mathbf{G}')\cdot\mathbf{r}'} \tag{3}$$

and to imaginary frequency,

(4) construction of the symmetrised dielectric matrix in reciprocal space

$$\tilde{\varepsilon}_{\mathbf{G}\mathbf{G}'}(\mathbf{k},\mathrm{i}\omega) = \delta_{\mathbf{G}\mathbf{G}'} - \frac{4\pi}{|\mathbf{k}+\mathbf{G}||\mathbf{k}+\mathbf{G}'|}P_{\mathbf{G}\mathbf{G}'}(\mathbf{k},\mathrm{i}\omega)\ , \tag{4}$$

(5) inversion of the symmetrised dielectric matrix for each $\mathbf{k}$-point and each imaginary frequency,

(6) calculation of the screened Coulomb interaction in reciprocal space

$$W_{\mathbf{G}\mathbf{G}'}(\mathbf{k},\mathrm{i}\omega) = \frac{4\pi}{|\mathbf{k}+\mathbf{G}||\mathbf{k}+\mathbf{G}'|}\tilde{\varepsilon}^{-1}_{\mathbf{G}\mathbf{G}'}(\mathbf{k},\mathrm{i}\omega)\ , \tag{5}$$

(7) Fourier transformation of W to imaginary time and to real space

$$W(\mathbf{r},\mathbf{r}';\mathrm{i}\tau) = \frac{1}{(2\pi)^3}\int_{\mathrm{BZ}}\mathrm{d}^3k\sum_{\mathbf{G},\mathbf{G}'}W_{\mathbf{G}\mathbf{G}'}(\mathbf{k},\mathrm{i}\tau)\mathrm{e}^{\mathrm{i}(\mathbf{k}+\mathbf{G})\cdot\mathbf{r}-\mathrm{i}(\mathbf{k}+\mathbf{G}')\cdot\mathbf{r}'}\ , \tag{6}$$

(8) computation of the self-energy in real space and imaginary time

$$\Sigma(\mathbf{r},\mathbf{r}';\mathrm{i}\tau) = \mathrm{i}G(\mathbf{r},\mathbf{r}';\mathrm{i}\tau)W(\mathbf{r},\mathbf{r}';\mathrm{i}\tau) \; . \tag{7}$$

The Coulomb singularity appears explicitly for $\mathbf{G} = \mathbf{0}$ or $\mathbf{G}' = \mathbf{0}$ as $\mathbf{k} \to \mathbf{0}$ in steps 4 and 6; in the actual implementation, however, it is treated in steps 5 and 7 for numerical reasons. The anisotropy enters the scheme naturally through the construction of the dielectric matrix and must be taken fully into account in the screened interaction.

The quasiparticle energies are obtained by computing the matrix elements of the self-energy $\langle\varphi_{n\mathbf{k}}|\Sigma(\mathrm{i}\tau)|\varphi_{n\mathbf{k}}\rangle$ on the imaginary time axis, which are then Fourier-transformed to imaginary frequency and analytically continued to the real frequency axis. Approximating the quasiparticle by the DFT Kohn-Sham wavefunctions finally gives the quasiparticle energies $\epsilon^{\mathrm{qp}}_{n\mathbf{k}}$ as solutions of the quasiparticle equation

$$\epsilon^{\mathrm{qp}}_{n\mathbf{k}} = \epsilon_{n\mathbf{k}} + \langle\varphi_{n\mathbf{k}}|\Sigma(\epsilon^{\mathrm{qp}}_{n\mathbf{k}}) - V_{\mathrm{xc}}|\varphi_{n\mathbf{k}}\rangle \; , \tag{8}$$

where V_{xc} is the exchange-correlation potential used in the underlying DFT calculation. The details of the analytic continuation and the solution of Equation (8) have been described elsewhere [20]. Self-consistency in GW would be achieved by entering step 2 with a new Green function obtained from solving Dyson's equation $G = G_0 + G_0\Sigma G$ after step 8 and iterating steps 2–8.

3 Treatment of the anisotropy

3.1 Anisotropy in the screened interaction

As shown in Appendix B the head ($\mathbf{G} = \mathbf{G}' = \mathbf{0}$) and the wings ($\mathbf{G} = \mathbf{0}$ or $\mathbf{G}' = \mathbf{0}$) of the dielectric matrix close to the Γ-point, i.e., for $\mathbf{k} \to \mathbf{0}$, depend on the direction in which this limit is taken. We denote this dependence by the spatial angle $\Omega_{\mathbf{k}}$, and the corresponding normalised direction vector by $\hat{\mathbf{k}}$. For simplicity, the imaginary frequency argument $\mathrm{i}\omega$ is omitted in the following. The directional dependence at the Γ-point is present in the whole inverse dielectric matrix, i.e., head, wings, and body. By block-wise inversion [28] it is easily shown that the head of the inverse symmetrised dielectric matrix takes the form (cf. Appendix B)

$$\tilde{\varepsilon}^{-1}_{\mathbf{00}}(\Omega_{\mathbf{k}}) = \frac{1}{\hat{\mathbf{k}}^{\mathrm{T}}\mathbf{L}\hat{\mathbf{k}}} \; , \tag{9}$$

where the matrix $\mathbf{L}$ is the macroscopic dielectric tensor. We note that in most other implementations, in which this anisotropy has been considered, such as [22,23], but not [21], the right-hand side of Equation (9) has been replaced by the expression $\hat{\mathbf{k}}^{\mathrm{T}}\mathbf{L}^{-1}\hat{\mathbf{k}}$ without formal justification.

Correspondingly, the wings can be expressed as

$$\tilde{\varepsilon}^{-1}_{\mathbf{G0}}(\Omega_{\mathbf{k}}) = -\tilde{\varepsilon}^{-1}_{\mathbf{00}}(\Omega_{\mathbf{k}})\left[\hat{\mathbf{k}}\cdot\mathbf{S}(\mathbf{G})\right] . \tag{10}$$

The vector $\mathbf{S}(\mathbf{G})$ is defined in Equation (B.15). For the remainder of this article we will restrict the discussion of the wings to the expression for $\mathbf{G}' = \mathbf{0}$ since the case $\mathbf{G} = \mathbf{0}$ is trivially obtained from the symmetry relation

$$\tilde{\varepsilon}^{-1}_{\mathbf{0G}'}(\Omega_{\mathbf{k}}) = [\tilde{\varepsilon}^{-1}_{\mathbf{G}'\mathbf{0}}(\Omega_{\mathbf{k}})]^* . \tag{11}$$

Finally, the body is given by

$$\tilde{\varepsilon}^{-1}_{\mathbf{GG}'}(\Omega_{\mathbf{k}}) = B^{-1}_{\mathbf{GG}'} + \tilde{\varepsilon}^{-1}_{\mathbf{00}}(\Omega_{\mathbf{k}})\left[\hat{\mathbf{k}}\cdot\mathbf{S}(\mathbf{G})\right]\left[\hat{\mathbf{k}}\cdot\mathbf{S}(\mathbf{G}')\right]^* , \tag{12}$$

where $\mathbf{B}$ denotes the body of the symmetrised dielectric matrix as defined in Equation (B.11). Expressions (9)-(12) imply that each element of the inverse dielectric matrix is, in general, not analytic at $\mathbf{k} = \mathbf{0}$, i.e., it does not have a unique limit for $\mathbf{k} \to \mathbf{0}$. This was already recognised more than 30 years ago by Pick et al. [28], but the treatment of this non-analytic behaviour in *GW* implementations has not been discussed widely in the literature. Hybertsen and Louie address the problem in the appendix of [15], but in the actual calculation they neglect the non-analytic part, arguing that the error can be made negligibly small with a sufficiently high number of $\mathbf{k}$-points. So far the anisotropy has only been considered for the head element in connection with the treatment of the Coulomb singularity [21,22,23]. We will return to this point later in Section 3.5.

Combining Equations (9) to (12) with Equation (5), we obtain the screened interaction for $\mathbf{k} \to \mathbf{0}$

$$W_{\mathbf{00}}(\mathbf{k}) \to \frac{4\pi}{|\mathbf{k}|^2}\tilde{\varepsilon}^{-1}_{\mathbf{00}}(\Omega_{\mathbf{k}}) , \tag{13}$$

$$W_{\mathbf{G0}}(\mathbf{k}) \to -\frac{4\pi}{|\mathbf{k}||\mathbf{G}|}\tilde{\varepsilon}^{-1}_{\mathbf{00}}(\Omega_{\mathbf{k}})\left[\hat{\mathbf{k}}\cdot\mathbf{S}(\mathbf{G})\right] , \tag{14}$$

$$W_{\mathbf{GG}'}(\mathbf{k}) \to \frac{4\pi}{|\mathbf{G}||\mathbf{G}'|}\left(B^{-1}_{\mathbf{GG}'} + \tilde{\varepsilon}^{-1}_{\mathbf{00}}(\Omega_{\mathbf{k}})\left[\hat{\mathbf{k}}\cdot\mathbf{S}(\mathbf{G})\right]\left[\hat{\mathbf{k}}\cdot\mathbf{S}(\mathbf{G}')\right]^*\right) . \tag{15}$$

The presence of the singularity at $\mathbf{G} = \mathbf{G}' = \mathbf{0}$ (Equation (13)) necessitates a special numerical treatment. In the space-time method, this problem is solved by splitting off a long-range part W^{lr} with the appropiate $\mathbf{k} \to \mathbf{0}$ behaviour, which is chosen such that its Fourier transform can be computed semi-analytically as described in detail in the following section. The remaining short-range part $W^{\mathrm{sr}} = W - W^{\mathrm{lr}}$ can then safely be treated numerically since it is no longer singular.

The next step in the space-time method is the Fourier transformation of W to real space (Equation (6)); in reciprocal-space algorithms it is the construction of the matrix elements of Σ. Both approaches involve an integration over the Brillouin zone after multiplication by an analytic function $a_{\mathbf{G}\mathbf{G}'}(\mathbf{k})$, and it is in this integration that the anisotropy must be taken into account. In practice, these integrals are usually discretised, which we express formally by partitioning the Brillouin zone into subzones Z_i with volume V_i:

$$\int_{\mathrm{BZ}} \mathrm{d}^3k \; W_{\mathbf{G}\mathbf{G}'}(\mathbf{k}) a_{\mathbf{G}\mathbf{G}'}(\mathbf{k}) = \sum_i \int_{\mathrm{Z}_i} \mathrm{d}^3k \; W_{\mathbf{G}\mathbf{G}'}(\mathbf{k}) a_{\mathbf{G}\mathbf{G}'}(\mathbf{k}) \; . \tag{16}$$

We denote the subzone that contains the Γ-point by Z_Γ and assume that it has inversion symmetry about $\mathbf{k} = \mathbf{0}$. While the subzone integrals for $i \neq \Gamma$ can be approximated by

$$\int_{\mathrm{Z}_i} \mathrm{d}^3k \; W_{\mathbf{G}\mathbf{G}'}(\mathbf{k}) a_{\mathbf{G}\mathbf{G}'}(\mathbf{k}) \approx V_i W_{\mathbf{G}\mathbf{G}'}(\mathbf{k}_i) a_{\mathbf{G}\mathbf{G}'}(\mathbf{k}_i) \; , \tag{17}$$

where $\mathbf{k}_i$ is a representative point for the subzone Z_i – usually its centre – the integrals over Z_Γ require a special treatment due to the non-analyticity of W at Γ.

In principle, even the singularity for $\mathbf{G} = \mathbf{G}' = \mathbf{0}$ can be treated in this way. Since it is illuminating to discuss existing isotropic and anisotropic singularity integration schemes in terms of approximations to an exact expression, we present the corresponding equations for reciprocal space algorithms in Section 3.5. In the space-time method, on the other hand, the separation into W^{lr} and W^{sr} is more efficient than the direct approach, because the analytic function $a_{\mathbf{G}\mathbf{G}'}(\mathbf{k})$ for the Fourier transformation

$$a_{\mathbf{G}\mathbf{G}'}(\mathbf{k}) = \mathrm{e}^{\mathrm{i}(\mathbf{k}+\mathbf{G})\cdot\mathbf{r} - \mathrm{i}(\mathbf{k}+\mathbf{G}')\cdot\mathbf{r}'} \tag{18}$$

depends on $\mathbf{r}$ and $\mathbf{r}'$ and would thus require the computation of the integrals over Z_Γ in Equation (16) for every $\mathbf{r}$ and $\mathbf{r}'$.

Since the long-range part of the interaction yields a significant contribution to the quasiparticle energies, an accurate treatment of its anisotropy is very important and is therefore described first in Section 3.2. In Section 3.3 we show that the apparent $1/|\mathbf{k}|$ singularity of the wings does not cause numerical problems for the integrals over Z_Γ, and in Section 3.4 the computation of the integrals for the body is presented.

3.2 Treatment of the head

In the space-time method the head of the inverse dielectric matrix is used to define the long-range part of the screened interaction. For this purpose, we extend Equation (13) to $\mathbf{G} = \mathbf{G}' \neq \mathbf{0}$ and define the long-range part for all $\mathbf{k}$ in the Brillouin zone as

$$W^{\mathrm{lr}}_{\mathbf{G}\mathbf{G}'}(\mathbf{k}) = \frac{4\pi}{(\mathbf{k}+\mathbf{G})^{\mathrm{T}}\mathbf{L}(\mathbf{k}+\mathbf{G})}\delta_{\mathbf{G}\mathbf{G}'} \ . \tag{19}$$

For numerical reasons we subtract the long-range part at the level of the inverse dielectric matrix after applying the body corrections described in Section 3.4 for $\mathbf{k} = \mathbf{0}$, and compute W^{sr} from this modified entity according to

$$\tilde{\varepsilon}^{-1,\mathrm{sr}}_{\mathbf{G}\mathbf{G}'}(\mathbf{k}) := \tilde{\varepsilon}^{-1}_{\mathbf{G}\mathbf{G}'}(\mathbf{k}) - \frac{|\mathbf{k}+\mathbf{G}|^2}{(\mathbf{k}+\mathbf{G})^{\mathrm{T}}\mathbf{L}(\mathbf{k}+\mathbf{G})}\delta_{\mathbf{G}\mathbf{G}'} \ , \tag{20}$$

$$W^{\mathrm{sr}}_{\mathbf{G}\mathbf{G}'}(\mathbf{k}) = \frac{4\pi}{|\mathbf{k}+\mathbf{G}||\mathbf{k}+\mathbf{G}'|}\tilde{\varepsilon}^{-1,\mathrm{sr}}_{\mathbf{G}\mathbf{G}'}(\mathbf{k}) \ . \tag{21}$$

By expanding the angular dependence of W^{lr} into spherical harmonics (cf. Appendix A)

$$W^{\mathrm{lr}}_{\mathbf{G}\mathbf{G}'}(\mathbf{k}) = \sum_{l=0}^{\infty}\sum_{m=-l}^{l} H_{lm}\frac{4\pi}{|\mathbf{k}+\mathbf{G}|^2}\delta_{\mathbf{G}\mathbf{G}'}Y_{lm}(\Omega_{\mathbf{k}+\mathbf{G}}) \ , \tag{22}$$

the Fourier transformation of W^{lr} can be performed analytically. Only even l contribute to the sum because the coefficients H_{lm} vanish for odd l. Making use of the expansion of a plane wave [29] in spherical harmonics Y_{lm} and spherical Bessel functions j_l,

$$\mathrm{e}^{\mathrm{i}\mathbf{k}\cdot\mathbf{r}} = 4\pi\sum_{l=0}^{\infty}\sum_{m=-l}^{l}\mathrm{i}^l j_l(kr)Y_{lm}(\Omega_{\mathbf{r}})Y^*_{lm}(\Omega_{\mathbf{k}}) \tag{23}$$

we arrive at

$$W^{\mathrm{lr}}(\mathbf{r},\mathbf{r}') = \sum_{l=0}^{\infty}\sum_{m=-l}^{l} c_l \mathrm{i}^l H_{lm} Y_{lm}(\Omega_{\mathbf{r}-\mathbf{r}'}) \frac{1}{|\mathbf{r}-\mathbf{r}'|} \ . \tag{24}$$

The coefficients c_l for even l are defined as

$$c_l = \frac{2}{\pi}\int_0^{\infty} \mathrm{d}x \ j_l(x) = \frac{(l-1)!!}{l!!} \tag{25}$$

with $n!! = n(n-2)(n-4)\cdots$. In practice we truncate the sum in Equation (24) at finite $l = l_{\max}$ (cf. Section 4.1).

For numerical convenience Σ is split into a static exchange part $\Sigma_{\mathrm{x}} = iGv$ and a frequency-dependent correlation part $\Sigma_{\mathrm{c}} = iG(W-v)$ in the space-time method [20]. This is achieved by subtracting the unscreened Coulomb interaction v from W^{lr} in its angular expansion (22), i.e., $1/\sqrt{4\pi}$ is subtracted from H_{00} for each imaginary frequency. Furthermore, the transformation from imaginary frequency to imaginary time is performed on the expansion coefficients $H_{lm}(\mathrm{i}\omega)$ directly, and we obtain $(W^{\mathrm{lr}} - v)$ according to Equation (24) with the expansion coefficients in imaginary time $H_{lm}(\mathrm{i}\tau)$.

A proper treatment of the anisotropy in the long-range part of the screened interaction is crucial to obtain converged results. This is easily illustrated in the space-time method: For non-local operators like W or Σ the density of the **k**-point sampling determines the range of the non-locality in real space. For example, a 4×4×4 **k**-grid corresponds to a maximum non-locality range or *interaction cell* of 4 real-space unit cells in each dimension. If parts of the long-range interaction remain in W^{sr} for small but finite **k**, the tails of W^{sr} extend over the boundary of the interaction cell and will be folded back in the numerical Fourier transformation when applying the periodic boundary conditions. Since the size of the interaction cell is determined by the **k**-point sampling, an inadequate treatment of the long-range part would result in an unsatisfactory **k**-convergence behaviour.

3.3 Treatment of the wings

The wings are antisymmetric with respect to **k**, i.e.,

$$W_{\mathbf{G0}}(\mathbf{k}) = -W_{\mathbf{G0}}(-\mathbf{k}) \ . \tag{26}$$

Hence we can write the Γ-point contribution as

$$
\begin{aligned}
&\int_{\mathrm{Z}_\Gamma} \mathrm{d}^3k \; W_{\mathbf{G0}}(\mathbf{k}) a_{\mathbf{G0}}(\mathbf{k}) \\
&= \frac{1}{2} \left(\int_{\mathrm{Z}_\Gamma} \mathrm{d}^3k \; W_{\mathbf{G0}}(\mathbf{k}) a_{\mathbf{G0}}(\mathbf{k}) + \int_{\mathrm{Z}_\Gamma} \mathrm{d}^3k \; W_{\mathbf{G0}}(-\mathbf{k}) a_{\mathbf{G0}}(-\mathbf{k}) \right) \\
&= -\frac{4\pi}{|\mathbf{G}|} \int_{\mathrm{Z}_\Gamma} \mathrm{d}^3k \; \tilde{\varepsilon}^{-1}_{\mathbf{00}}(\Omega_\mathbf{k}) \left[\hat{\mathbf{k}} \cdot \mathbf{S}(\mathbf{G}) \right] \left[\hat{\mathbf{k}} \cdot \nabla_\mathbf{k} a_{\mathbf{G0}}(\Omega_\mathbf{k})|_{\mathbf{k}=\mathbf{0}} + \mathrm{O}(|\mathbf{k}|^2) \right] \; , \qquad (27)
\end{aligned}
$$

where we have made use of the Taylor expansion of the analytic function $a_{\mathbf{G0}}(\mathbf{k})$. The important benefit of this reformulation is that no term in the integrand is singular, and therefore we do not expect any numerical difficulties close to the Γ-point. This applies equally to the Fourier transformation in the space-time method as well as to the construction of the self-energy in reciprocal-space approaches.

In practice we neglect the wing contributions from the Γ-point in the Fourier transformation, because evaluating Equation (27) for each $\mathbf{r}$ and $\mathbf{r}'$ would be computationally very demanding. The associated error scales as V_Γ. It is thus automatically controlled by the standard $\mathbf{k}$-point convergence tests, since V_Γ is inversely proportional to the number of points in our regular $\mathbf{k}$-point grid. Test calculations indicate that the overall convergence behaviour shows no significant improvement for a more sophisticated treatment of the wings. We note that in contrast to head and body the isotropic average for the wing contribution vanishes, i.e., no analytic contribution has to be considered when the non-analytic part is neglected.

3.4 Treatment of the body

For $|\mathbf{k}| \ll |\mathbf{G}|$ we see from Equation (18) that we can approximate $a_{\mathbf{GG'}}(\mathbf{k}) \approx a_{\mathbf{GG'}}(\mathbf{0})$. Similar considerations apply to the analytic function in reciprocal-space approaches. We can then express

$$
\int_{\mathrm{Z}_\Gamma} \mathrm{d}^3k \; W_{\mathbf{GG'}}(\mathbf{k}) a_{\mathbf{GG'}}(\mathbf{k}) \approx a_{\mathbf{GG'}}(\mathbf{0}) \int_{\mathrm{Z}_\Gamma} \mathrm{d}^3k \; \frac{4\pi \tilde{\varepsilon}^{-1}_{\mathbf{GG'}}(\Omega_\mathbf{k})}{|\mathbf{G}||\mathbf{G'}|} \qquad (28)
$$

as a discretised contribution analogous to Equation (17) with an averaged anisotropy

$$
\tilde{\varepsilon}^{-1}_{\mathbf{GG'}}(\mathbf{0}) := \frac{1}{V_\Gamma} \int_{\mathrm{Z}_\Gamma} \mathrm{d}^3k \; \tilde{\varepsilon}^{-1}_{\mathbf{GG'}}(\Omega_\mathbf{k}) \; . \qquad (29)
$$

We will now show how this average can be computed efficiently. To this end we rewrite the integral in polar coordinates as

$$\tilde{\varepsilon}^{-1}_{\mathbf{G}\mathbf{G}'}(\mathbf{0}) = \int \mathrm{d}\Omega_{\mathbf{k}}\; w(\Omega_{\mathbf{k}}) \tilde{\varepsilon}^{-1}_{\mathbf{G}\mathbf{G}'}(\Omega_{\mathbf{k}}) \quad \text{with} \quad w(\Omega_{\mathbf{k}}) = \frac{1}{V_\Gamma} \int_0^{k_{\max}(\Omega_{\mathbf{k}})} k^2 \,\mathrm{d}k \;, \quad (30)$$

where $k_{\max}(\Omega_{\mathbf{k}})$ is the distance from the centre to the surface of Z_Γ in the direction of $\Omega_{\mathbf{k}}$, and $w(\Omega_{\mathbf{k}})$ acts as an angular weight function that takes the shape of the Γ-zone element into account and may be subject to additional approximations, e.g., for spherical averages it is simply a constant $w(\Omega_{\mathbf{k}}) = 1/4\pi$.

Inserting Equation (12), we obtain a very simple expression

$$\begin{aligned}\tilde{\varepsilon}^{-1}_{\mathbf{G}\mathbf{G}'}(\mathbf{0}) = B^{-1}_{\mathbf{G}\mathbf{G}'} + \sum_{l=0}^{\infty} \sum_{m=-l}^{l} \sum_{m'=-1}^{1} \sum_{m''=-1}^{1} \overline{H}_{lm} S_{m'}(\mathbf{G}) S^*_{m''}(\mathbf{G}') \\ \times \int \mathrm{d}\Omega_{\mathbf{k}}\; Y_{lm}(\Omega_{\mathbf{k}}) Y_{1m'}(\Omega_{\mathbf{k}}) Y^*_{1m''}(\Omega_{\mathbf{k}}) \end{aligned} \quad (31)$$

when expanding $[w(\Omega_{\mathbf{k}})\tilde{\varepsilon}^{-1}_{\mathbf{00}}(\Omega_{\mathbf{k}})]$ as well as $\hat{\mathbf{k}} \cdot \mathbf{S}(\mathbf{G})$ in spherical harmonics as described in Appendix A. The angular integrals in Equation (31) are nothing but the Clebsch–Gordan coefficients for the spherical harmonics $(lm\; 1m'|1m'')$. From the properties of the Clebsch–Gordan coefficients [30] it follows that only a small number of non-zero terms contribute to Equation (31), namely $l = 0$ with 3 terms and $l = 2$ with 9 terms. We refer to these 12 terms as "body corrections". In the original space-time implementation [20], Equation (12) was averaged over the Cartesian directions, which is equivalent to including only the $l = 0$ terms with an approximate coefficient $\overline{H}_{00}$, calculated with the spherical weight function $w(\Omega) = 1/4\pi$ and a 3-point integration. We note that the exact procedure includes only 9 more terms with $l = 2$.

3.5 Treatment of the anisotropy in reciprocal-space approaches

For completeness, we present here a simple recipe to take the anisotropy into account in reciprocal-space approaches. The analytic function that appears in the computation of, e.g., the self-energy matrix element $\langle \phi_{n\mathbf{q}} | \Sigma(\omega') | \phi_{n\mathbf{q}} \rangle$ is given by an expression of the form

$$a_{\mathbf{G}\mathbf{G}'}(\mathbf{k}) = \int \mathrm{d}^3 q \sum_m [M^{mn}_{\mathbf{G}}(\mathbf{q}, \mathbf{k})]^* M^{mn}_{\mathbf{G}'}(\mathbf{q}, \mathbf{k}) F(\omega, \omega', \epsilon_{m\mathbf{q}-\mathbf{k}}) \;, \quad (32)$$

where $M^{mn}_{\mathbf{G}}(\mathbf{q},\mathbf{k}) = \langle \phi_{n\mathbf{q}-\mathbf{k}} | e^{-\mathrm{i}(\mathbf{k}+\mathbf{G})\mathbf{r}} | \phi_{n\mathbf{q}} \rangle$ and $F(\omega, \omega', \epsilon_{m(\mathbf{q}-\mathbf{k})})$ contains prefactors and frequency integrals [11]. For body and wings the approach outlined in the previous sections also applies for this analytic function. For the head element, on the other hand, the integral to compute is

$$\int_{\mathrm{Z}_\Gamma} \mathrm{d}^3k \; \frac{a_{\mathbf{00}}(\mathbf{k})}{\mathbf{k}^{\mathrm{T}}\mathbf{L}\mathbf{k}} \; , \tag{33}$$

where $a_{\mathbf{00}}(\mathbf{k})$ is analytic at $\mathbf{k} = \mathbf{0}$. Assuming that $a_{\mathbf{00}}(\mathbf{k})$ is non-zero and varies sufficiently slowly with $\mathbf{k}$, we set $a_{\mathbf{00}}(\mathbf{k}) \approx a_{\mathbf{00}}(\mathbf{0})$ and evaluate the remaining integral in polar coordinates

$$\int_{\mathrm{Z}_\Gamma} \mathrm{d}^3k \; \frac{a_{\mathbf{00}}(\mathbf{0})}{\mathbf{k}^{\mathrm{T}}\mathbf{L}\mathbf{k}} = a_{\mathbf{00}}(\mathbf{0}) \int \mathrm{d}\Omega_{\mathbf{k}} \; \frac{1}{\hat{\mathbf{k}}^{\mathrm{T}}\mathbf{L}\hat{\mathbf{k}}} \int_0^{k_{\max}(\Omega_{\mathbf{k}})} k^2 \mathrm{d}k \; \frac{1}{k^2} \; . \tag{34}$$

In accordance with the computation of $\overline{H}_{00}$ as described in Appendix A, the angular integral can be computed numerically on an appropriate angular grid with the angular weight function

$$K(\Omega_{\mathbf{k}}) = \int_0^{k_{\max}(\Omega_{\mathbf{k}})} k^2 \mathrm{d}k \; \frac{1}{k^2} = k_{\max}(\Omega_{\mathbf{k}}) \; . \tag{35}$$

Alternatively, but formally equivalent, $K(\Omega_{\mathbf{k}})$ can be expanded in spherical harmonics with coefficients K_{lm}. The integral then becomes

$$\int_{\mathrm{Z}_\Gamma} \mathrm{d}^3k \; \frac{a_{\mathbf{00}}(\mathbf{0})}{\mathbf{k}^{\mathrm{T}}\mathbf{L}\mathbf{k}} = a_{\mathbf{00}}(\mathbf{0}) \sum_{l=0}^{\infty} \sum_{m=-l}^{l} K^*_{lm} H_{lm} \; . \tag{36}$$

Equation (36) is conducive for a discussion of different anisotropy and the Coulomb singularity treatments. In all isotropic approximations the sum over l and m is restricted to the $l = 0, m = 0$ term. In the "spherical" approximation [31] used in the early days of modern GW calculations [15,32] K_{00} is further replaced by a shape-independent term

$$K^{\mathrm{sph}}_{00} = \frac{1}{Y_{00}} \left(\int \mathrm{d}\Omega \; k^3_{\max}(\Omega) \right)^{1/3} \; . \tag{37}$$

The numerical computation of H_{00} is restricted to 3 angular points if the average over the Cartesian directions is taken, which might introduce an additional inaccuracy for anisotropic systems. In the improved integration scheme

used by Pulci et al. [22] as well as in the integration scheme by Wenzien et al. [23], the head of the inverse dielectric matrix is written as a tensor and hence includes also the $l = 2$ terms (cf. Appendix A). The tensor itself is chosen to reproduce the correct value in the main directions, so H_{lm} is effectively determined from three independent points only. In the scheme that we propose here only the choice of the angular grid determines the accuracy of the sum in Equation (36). It should be comparable to the scheme proposed by Hott [21], which formally includes all terms and also involves a numerical integration, the details of which are unfortunately not specified in [21]. Similarly, the offset-Γ-point method described in [11] in principle allows to capture the anisotropy to arbitrary precision. However, the accuracy with which this is achieved in practice depends on the choice of **k**-points.

4 Results

The equations presented in the previous sections were implemented into the `gwst` code [20,27]. The test system was chosen to be a periodically repeated 4-layer Si(001) slab saturated with hydrogen and a vacuum separation between the Si surface atoms equivalent to 4 layers. 15 points per half-axis were used both for the imaginary time and frequency Gauss–Legendre grids at a maximum numerical range of 6 atomic units. Convergence in the plane-wave cutoff is achieved for 7 Hartree, and unoccupied states up to 5 Hartree above the Fermi energy were included (610 bands). Head and wings were computed separately with a **k**-point grid of $14 \times 14 \times 1$ and 120 bands. These parameters are sufficient to obtain quasiparticle energies converged to within 0.05 eV.

Taking the body corrections from Equation (31) into account changes the quasiparticle energies of our test system only little compared to neglecting them completely and setting $\tilde{\varepsilon}^{-1}_{\mathbf{GG}'}(\mathbf{0}) = B^{-1}_{\mathbf{GG}'}$. The magnitude of the corrections depends on the weight of the Γ-point and hence on the **k**-point sampling, amounting to ∼10 meV for a $3 \times 3 \times 1$ sampling and 1–2 meV for $8 \times 8 \times 1$. While these corrections are small compared to the accuracy of our test calculation, they might be larger for systems with stronger local-field effects. Since the additional computational effort is small we always include them.

The repeated-slab arrangement considered here is a hypothetical system, that, at least until now, cannot be prepared in experiment. However, since it is fundamentally a strongly anisotropic system, it provides an ideal test case for our modifications. It also provides the possibility to tune the degree of anisotropy by varying the slab thickness and the separation. If the slab separation were increased to infinity, the limit of an isolated slab would be recovered. If additionally the slab thickness were taken to infinity the limit of a hydrogenated silicon surface would be reached. For the present choice of slab thickness and

Table 1
Dependence of the quasiparticle energies (in eV relative to the valence-band maximum) on the maximum angular momentum l in Equation (24). The **k**-point sampling for the data presented here is $4 \times 4 \times 4$. Other samplings show the same behaviour.

$l_{\max}$	0	2	4	6
lowest valence state	−10.448	−10.338	−10.336	−10.336
lowest conduction state	3.560	3.424	3.409	3.410

separation, the non-zero elements of the dielectric tensor, including local-field effects and the contributions of the non-local pseudopotential (cf. Appendix C), are ε_{xx}=5.1, ε_{yy}=5.5, and ε_{zz}=2.2 at the smallest imaginary frequency ω=0.036 Hartree, in agreement with effective-medium theory. Without the contributions of the non-local pseudopotential the values are ε_{xx}=5.9, ε_{yy}=6.5, and ε_{zz}=2.8, which underlines their importance for our test system. Varying the thickness or the separation produces changes in the quasiparticle energies that are of similar magnitude as the errors from an inadequate treatment of the anisotropy. In order to be able to investigate the surface or isolated-film limit, it hence proved to be essential to take the anisotropy modifications into account [33].

4.1 Convergence with respect to $l_{\max}$

In Table 1 we report the convergence of the quasiparticle energies with respect to the maximum value of l used for the evaluation of W^{lr} in real space according to Equation (24). It can be seen that already with $l_{\max} = 2$ the results lie within our level of accuracy ($\sim 0.05\,\mathrm{eV}$), and with $l_{\max} = 4$ absolute convergence is reached. These results also indicate that previous approaches [22,23], which have treated the anisotropy at the level of $l_{\max} = 2$, have incorporated the most important aspects of the anisotropy since the terms from $l > 2$ yield only minor corrections. Nevertheless, as the computational cost for evaluating higher terms in Equation (24) is negligible, we use $l_{\max} = 6$ in practice.

4.2 Convergence behaviour with respect to **k***-points*

In Figure 1 we show the convergence with respect to the number of **k**-points in the direction perpendicular to the surface for the quasiparticle energy of the lowest conduction state. Other states exhibit a similar behaviour. It is obvious that the original isotropic averaging for the screened interaction, notably in the long-range part, leads to an unphysical linear increase in the quasiparticle energy. In contrast, the anisotropic treatment converges rapidly.

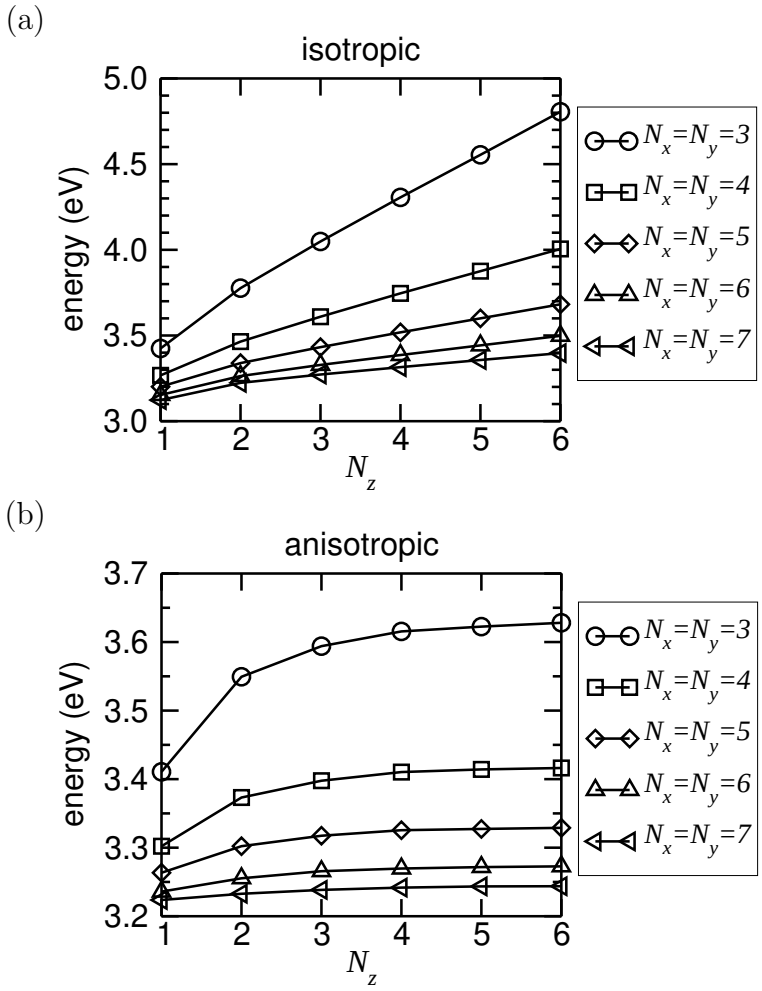

Fig. 1. Convergence of the lowest conduction-band energy with respect to the number of k-points N_z perpendicular to the surface for (a) the original isotropic implementation and (b) with the anisotropy taken into account. The quantitative behaviour depends on the sampling in the parallel direction ($N_x = N_y$). Note the different scales of the two graphs.

The reason for the linear increase in the isotropic treatment is found in the inadequate treatment of the singularity, which is not fully removed. Integrating $1/|\mathbf{k}|^2$ numerically yields for $k_x = k_y = 0$ with $\Delta k_z = k_{\max}/N_z$

$$\sum_{n=1}^{N_z} \Delta k_z \frac{1}{(n\Delta k_z)^2} \longrightarrow \int_{\Delta k_z}^{k_{\max}} \mathrm{d}k \, \frac{1}{k^2} = \frac{1}{\Delta k_z} - \frac{1}{k_{\max}} = \frac{N_z - 1}{k_{\max}} \tag{38}$$

and hence a linearly diverging contribution, whose weight is proportional to $\Delta k_x \Delta k_y \sim (N_x N_y)^{-1}$. When the **k**-sampling is increased in all three directions simultaneously, no such linear divergence occurs, as can be seen from the three-dimensional plot in Figure 2 when going from the left side (small N_x, N_y, N_z) to the right. However, such a restriction is undesirable and ineffi-

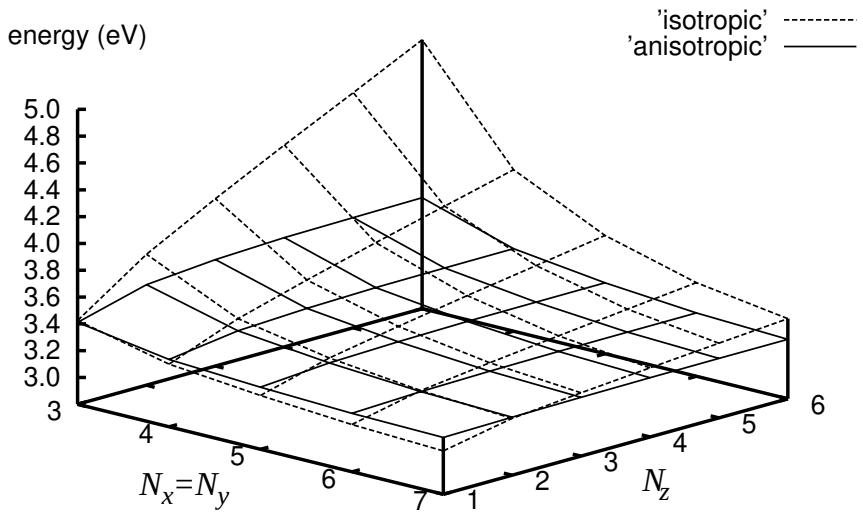

Fig. 2. Convergence of the lowest conduction-band state in the isotropic and anisotropic treatment for various **k**-meshes.

Table 2
Extrapolated $\Delta k_x = \Delta k_y \to 0$ quasiparticle energies in eV for the lowest conduction state for the isotropic and anisotropic treatment with a fixed number of **k**-points in the z-direction N_z.

N_z	1	2	3	4	5	6
isotropic	3.063	3.094	3.090	3.082	3.074	3.064
anisotropic	3.179	3.160	3.158	3.157	3.157	3.156

cient in practice. Therefore, only the proper anisotropic treatment enables us to investigate the importance of the **k**-point sampling in the direction perpendicular to the surface, which is directly related to the interaction with adjacent slabs in GW calculations [33]. To our knowledge, the convergence in the perpendicular direction has not been addressed in previous GW calculations for slab systems, probably under the erroneous assumption that neighbouring slabs do not interact.

The computed quasiparticle energies appear to be a linear function of the product $\Delta k_x \Delta k_y$ when N_z is kept fixed (not shown). This can be exploited to extrapolate the value for $\Delta k_x = \Delta k_y \to 0$, as shown in table 2. The extrapolated values evidently depend much less on the number of **k**-points in the z-direction than those for finite Δk_x and Δk_y. For isotropic averaging, the situation greatly improves after extrapolation, but a small, systematic trend towards lower energies for larger N_z is still present. This indicates that even after extrapolation no reliable convergence with respect to the number of **k**-points can be reached in the isotropic case. A comparison with the anisotropic treatment shows that the absolute error of the isotropic averaging is about 0.1 eV, larger than could have been estimated from the isotropic data alone.

5 Summary

We have presented a comprehensive account of the treatment of anisotropic screening in *GW* calculations that employ reciprocal space for the computation of the screened interaction. In particular, we have demonstrated that this requires only small modifications of the original *GW* space-time implementation [20]. The additional terms are computationally not very demanding. Furthermore, we have shown that the treatment of the anisotropy in other *GW* implementations can be understood in terms of approximations to the exact equations.

The improvements presented in this article greatly increase the efficiency of *GW* calculations for anisotropic systems in the space-time method, e.g., for films and surfaces. This is mostly due to the fact that the fully anisotropic treatment enables us to converge the **k**-point sampling in the perpendicular and parallel direction separately, whereas isotropic averaging leads to an unacceptable linear divergence in this case. The number of **k**-points required for converged results is thus reduced considerably.

Acknowledgements

We thank Lucia Reining, Fabien Bruneval, Francesco Sottile, Carlo Rozzi, Hardy Gross, Angel Rubio, and Christoph Friedrich for fruitful discussions. This work was funded in part by the EU through the Nanophase Research Training Network (Contract No. HPRN-CT-2000-00167) and the Nanoquanta Network of Excellence (Contract No. NMP-4-CT-2004-500198). Philipp Eggert acknowledges the Deutscher Akademischer Austauschdienst for financial support.

A Angular expansion of vector expressions

In this section we briefly summarise how simple expressions for a normalised vector $\hat{\mathbf{k}}$ can be written in terms of spherical harmonics of the corresponding spatial angle $\Omega_{\mathbf{k}}$. The expansion of a scalar product $\hat{\mathbf{k}} \cdot \mathbf{r}$ requires spherical harmonics of order $l = 1$

$$\hat{\mathbf{k}} \cdot \mathbf{r} = \sum_{m=-1}^{1} r_m Y_{1m}(\Omega_{\mathbf{k}}) \tag{A.1}$$

with

$$r_0 = \sqrt{\frac{4\pi}{3}} r_z \ , \quad r_{\pm 1} = \sqrt{\frac{2\pi}{3}} (\mp r_x + \mathrm{i} r_y) \ . \tag{A.2}$$

It is also straightforward to show that a tensor expression $\hat{\mathbf{k}}^{\mathrm{T}} \mathbf{L} \hat{\mathbf{k}}$, where $\mathbf{L}$ is symmetric, can be written in terms of spherical harmonics up to l=2 as

$$\hat{\mathbf{k}}^{\mathrm{T}} \mathbf{L} \hat{\mathbf{k}} = \sum_{l \in \{0,2\}} \sum_{m=-l}^{l} L_{lm} Y_{lm}(\Omega_{\mathbf{k}}) \tag{A.3}$$

with the coefficients

$$\begin{aligned} L_{00} &= \sqrt{\frac{4\pi}{9}} (L_{xx} + L_{yy} + L_{zz}) \ , \qquad L_{20} = \sqrt{\frac{4\pi}{45}} (2L_{zz} - L_{xx} - L_{yy}) \ , \\ L_{2,\pm 1} &= \sqrt{\frac{8\pi}{15}} (\mp L_{xz} + \mathrm{i} L_{yz}) \ , \qquad L_{2,\pm 2} = \sqrt{\frac{2\pi}{15}} (L_{xx} - L_{yy} \mp 2\mathrm{i} L_{xy}) \ . \end{aligned} \tag{A.4}$$

In the *GW* space-time method the term $\hat{\mathbf{k}}^{\mathrm{T}} \mathbf{L} \hat{\mathbf{k}}$ appears in the denominator of the head element of the inverse dielectric matrix (9) as well as its product with an angular weight function $w(\Omega_{\mathbf{k}})$. In order to expand these expressions in spherical harmonics

$$\frac{1}{\hat{\mathbf{k}}^{\mathrm{T}} \mathbf{L} \hat{\mathbf{k}}} = \sum_{l=0}^{\infty} \sum_{m=-l}^{l} H_{lm} Y_{lm}(\Omega_{\mathbf{k}}) \ , \tag{A.5}$$

$$\frac{w(\Omega_{\mathbf{k}})}{\hat{\mathbf{k}}^{\mathrm{T}} \mathbf{L} \hat{\mathbf{k}}} = \sum_{l=0}^{\infty} \sum_{m=-l}^{l} \overline{H}_{lm} Y_{lm}(\Omega_{\mathbf{k}}) \ , \tag{A.6}$$

we determine the coefficients numerically by performing the following integrals on a Lebedev–Laikov grid [34]

$$H_{lm} = \int \mathrm{d}\Omega_{\mathbf{k}} \ Y^*_{lm}(\Omega_{\mathbf{k}}) \frac{1}{\hat{\mathbf{k}}^{\mathrm{T}} \mathbf{L} \hat{\mathbf{k}}} \ , \tag{A.7}$$

$$\overline{H}_{lm} = \int \mathrm{d}\Omega_{\mathbf{k}} \ Y^*_{lm}(\Omega_{\mathbf{k}}) \frac{w(\Omega_{\mathbf{k}})}{\hat{\mathbf{k}}^{\mathrm{T}} \mathbf{L} \hat{\mathbf{k}}} \ . \tag{A.8}$$

Since $\mathbf{k}^{\mathrm{T}} \mathbf{L} \mathbf{k}$ and $w(\Omega_{\mathbf{k}})$ are even functions, only even l-components contribute to the sums.

B Dielectric matrix

For calculating the long-range limit of the symmetrised dielectric matrix we follow the derivation of Baroni and Resta [35]. For $\mathbf{k} \to \mathbf{0}$ we have

$$P_{\mathbf{00}}(\mathbf{k}) \sim |k|^2 \qquad \text{“head”}, \tag{B.1}$$
$$P_{\mathbf{G0}}(\mathbf{k}) \sim |k| \qquad \text{“wing”}, \tag{B.2}$$
$$P_{\mathbf{GG'}}(\mathbf{k}) \qquad \text{“body”} \ . \tag{B.3}$$

This behaviour holds even for the exact polarisability of a non-metallic system and cancels the Coulomb singularity in the symmetrised dielectric matrix. In the context of the GW approximation Equations (B.1) to (B.3) are also valid for full self-consistency. However, here we restrict ourselves to the non-self-consistent case and derive expressions for the corresponding Taylor coefficients from the Adler–Wiser formula [36,37] for the polarisability

$$\begin{aligned} P_{\mathbf{GG'}}(\mathbf{k}, \mathrm{i}\omega) = -\frac{4}{(2\pi)^3} \sum_{v,c} \int \mathrm{d}^3 q \ \frac{\epsilon_{c\mathbf{q}+\mathbf{k}} - \epsilon_{v\mathbf{q}}}{(\epsilon_{c\mathbf{q}+\mathbf{k}} - \epsilon_{v\mathbf{q}})^2 + \omega^2} \\ \times \left\langle \varphi_{v\mathbf{q}} \middle| e^{-\mathrm{i}(\mathbf{k}+\mathbf{G})\cdot\mathbf{r}} \middle| \varphi_{c\mathbf{q}+\mathbf{k}} \right\rangle \left\langle \varphi_{c\mathbf{q}+\mathbf{k}} \middle| e^{\mathrm{i}(\mathbf{k}+\mathbf{G'})\cdot\mathbf{r}} \middle| \varphi_{v\mathbf{q}} \right\rangle \ , \end{aligned} \tag{B.4}$$

where the sum over v and c runs over occupied and unoccupied states, respectively. For $\mathbf{G'} = \mathbf{0}$ and $\mathbf{k} \to \mathbf{0}$ this leads to

$$\begin{aligned} P_{\mathbf{G0}}(\mathbf{k}, \mathrm{i}\omega) \to -\frac{4\mathrm{i}}{(2\pi)^3} \sum_{v,c} \int \mathrm{d}^3 q \ \frac{\epsilon_{c\mathbf{q}} - \epsilon_{v\mathbf{q}}}{(\epsilon_{c\mathbf{q}} - \epsilon_{v\mathbf{q}})^2 + \omega^2} \\ \times \left\langle \varphi_{v\mathbf{q}} \middle| e^{-\mathrm{i}\mathbf{G}\cdot\mathbf{r}} \middle| \varphi_{c\mathbf{q}} \right\rangle (\mathbf{k} \cdot \langle \varphi_{c\mathbf{q}} | \mathbf{r} | \varphi_{v\mathbf{q}} \rangle) \ , \end{aligned} \tag{B.5}$$

while for $\mathbf{G} = \mathbf{G'} = \mathbf{0}$ and $\mathbf{k} \to \mathbf{0}$ the result is

$$\begin{aligned} P_{\mathbf{00}}(\mathbf{k}, \mathrm{i}\omega) \to -\frac{4}{(2\pi)^3} \sum_{v,c} \int \mathrm{d}^3 q \ \frac{\epsilon_{c\mathbf{q}} - \epsilon_{v\mathbf{q}}}{(\epsilon_{c\mathbf{q}} - \epsilon_{v\mathbf{q}})^2 + \omega^2} \\ \times (\mathbf{k} \cdot \langle \varphi_{v\mathbf{q}} | \mathbf{r} | \varphi_{c\mathbf{q}} \rangle) (\mathbf{k} \cdot \langle \varphi_{c\mathbf{q}} | \mathbf{r} | \varphi_{v\mathbf{q}} \rangle) \ . \end{aligned} \tag{B.6}$$

The computation of the matrix elements $\langle * | \mathbf{r} | * \rangle$ for the Kohn–Sham eigenfunctions is presented in Appendix C. Writing the scalar products $\mathbf{k} \cdot \langle * | \mathbf{r} | * \rangle$ as $\sum_\alpha k_\alpha \langle * | r_\alpha | * \rangle$, where α runs over the spatial (Cartesian) directions, we arrive at the following expressions for the wings of the symmetrised dielectric matrix in terms of a new vector quantity $\mathbf{U}(\mathbf{G}, \omega)$:

$$\tilde{\varepsilon}_{\mathbf{G0}}(\mathbf{k}, \mathrm{i}\omega) \to \sum_\alpha \frac{k_\alpha}{|\mathbf{k}|} \frac{16\pi i}{(2\pi)^3 |\mathbf{G}|} \sum_{v,c} \int \mathrm{d}^3 q \ \frac{\epsilon_{c\mathbf{q}} - \epsilon_{v\mathbf{q}}}{(\epsilon_{c\mathbf{q}} - \epsilon_{v\mathbf{q}})^2 + \omega^2} \tag{B.7}$$

$$\times \left\langle \varphi_{v\mathbf{q}} \middle| e^{-\mathrm{i}\mathbf{G}\cdot\mathbf{r}} \middle| \varphi_{c\mathbf{q}} \right\rangle \langle \varphi_{c\mathbf{q}} | r_\alpha | \varphi_{v\mathbf{q}} \rangle$$
$$=: \sum_\alpha \frac{k_\alpha}{|\mathbf{k}|} U_\alpha(\mathbf{G}, \omega) \tag{B.8}$$

and analogously for the head element in terms of a new tensor quantity $\mathrm{F}(\omega)$

$$\tilde{\varepsilon}_{\mathbf{00}}(\mathbf{k}, \mathrm{i}\omega) \to 1 + \sum_{\alpha,\beta} \frac{k_\alpha k_\beta}{|\mathbf{k}|^2} \frac{16\pi}{(2\pi)^3} \sum_{v,c} \int \mathrm{d}^3 q \; \frac{\epsilon_{c\mathbf{q}} - \epsilon_{v\mathbf{q}}}{(\epsilon_{c\mathbf{q}} - \epsilon_{v\mathbf{q}})^2 + \omega^2} \tag{B.9}$$
$$\times \langle \varphi_{v\mathbf{q}} | r_\alpha | \varphi_{c\mathbf{q}} \rangle \langle \varphi_{c\mathbf{q}} | r_\beta | \varphi_{v\mathbf{q}} \rangle$$
$$=: \sum_{\alpha,\beta} \frac{k_\alpha k_\beta}{|\mathbf{k}|^2} F_{\alpha\beta}(\omega) \; . \tag{B.10}$$

Since for many systems head and wings converge much slower with respect to the $\mathbf{k}$-point sampling, but faster with respect to the number of conduction bands compared to the body [35], we compute them in a separate calculation. Equations (B.8) and (B.10) hold also for the self-consistent case, but the coefficients $U_\alpha(\mathbf{G}; \omega)$ and $F_{\alpha\beta}(\omega)$ would have to be computed differently. The considerations following from now on then apply to self-consistent GW, too.

Equations (B.8) and (B.10) illustrate that the limit for $\mathbf{k} \to \mathbf{0}$ is finite but will, in general, depend on the direction $\mathbf{k}/|\mathbf{k}| = \hat{\mathbf{k}}$ in which the Γ-point is approached. We denote this directional dependence in the limit $\mathbf{k} = \mathbf{0}$ by the directional (spatial) angle $\Omega_\mathbf{k}$. In existing implementations the treatment of the directional dependence varies. Sometimes, the direction $\Omega_\mathbf{k}$ is simply fixed to a single value. It is also common to carry the directional dependence through the inversion by performing a block-wise inversion [28], which is also the approach taken in the original space-time implementation [20]. For brevity, we omit the frequency argument from the following derivation. We denote the body of the symmetrised dielectric matrix ($\mathbf{G} \neq 0, \mathbf{G}' \neq 0$) at $\mathbf{k} = \mathbf{0}$ by $\mathbf{B}$, the wings by $\mathbf{w}$ (a column vector) and $\mathbf{w}^\dagger$ (a row vector), and the head by H. The symmetrised dielectric matrix hence takes the form

$$\tilde{\varepsilon}(\Omega_\mathbf{k}) = \begin{pmatrix} H(\Omega_\mathbf{k}) & \mathbf{w}^\dagger(\Omega_\mathbf{k}) \\ \mathbf{w}(\Omega_\mathbf{k}) & \mathbf{B} \end{pmatrix} \; . \tag{B.11}$$

Head, wings, and body of the symmetrised inverse dielectric matrix are then given by [28]

$$\tilde{\varepsilon}^{-1}_{\mathbf{00}}(\Omega_\mathbf{k}) = \Big[H(\Omega_\mathbf{k}) - \sum_{\mathbf{G},\mathbf{G}' \neq \mathbf{0}} w^*_\mathbf{G}(\Omega_\mathbf{k}) B^{-1}_{\mathbf{G}\mathbf{G}'} w_{\mathbf{G}'}(\Omega_\mathbf{k}) \Big]^{-1} \; , \tag{B.12}$$

$$\tilde{\varepsilon}^{-1}_{\mathbf{G0}}(\Omega_\mathbf{k}) = -\tilde{\varepsilon}^{-1}_{\mathbf{00}}(\Omega_\mathbf{k}) \sum_{\mathbf{G}' \neq \mathbf{0}} B^{-1}_{\mathbf{G}\mathbf{G}'} w_{\mathbf{G}'}(\Omega_\mathbf{k}) \; , \tag{B.13}$$

$$\tilde{\varepsilon}^{-1}_{\mathbf{G}\mathbf{G}'}(\Omega_{\mathbf{k}}) = B^{-1}_{\mathbf{G}\mathbf{G}'} + \tilde{\varepsilon}^{-1}_{\mathbf{0}\mathbf{0}}(\Omega_{\mathbf{k}})\Big[\sum_{\mathbf{G}''\neq\mathbf{0}} B^{-1}_{\mathbf{G}\mathbf{G}''} w_{\mathbf{G}''}(\Omega_{\mathbf{k}})\Big] \times\Big[\sum_{\mathbf{G}''\neq\mathbf{0}} w^{*}_{\mathbf{G}''}(\Omega_{\mathbf{k}}) B^{-1}_{\mathbf{G}''\mathbf{G}'}\Big] . \tag{B.14}$$

Using equation (B.8), we now define the auxiliary vector

$$S_{\alpha}(\mathbf{G}) = \sum_{\mathbf{G}'\neq\mathbf{0}} B^{-1}_{\mathbf{G}\mathbf{G}'} U_{\alpha}(\mathbf{G}') \tag{B.15}$$

and rewrite equation (B.12) as

$$\tilde{\varepsilon}^{-1}_{\mathbf{0}\mathbf{0}}(\Omega_{\mathbf{k}}) = \Big[\sum_{\alpha,\beta} \hat{k}_{\alpha}\hat{k}_{\beta}\Big(F_{\alpha\beta} - \sum_{\mathbf{G}\neq\mathbf{0}} U^{*}_{\alpha}(\mathbf{G}) S_{\beta}(\mathbf{G})\Big)\Big]^{-1} =: \frac{1}{\hat{\mathbf{k}}^{\mathrm{T}}\mathbf{L}\hat{\mathbf{k}}} , \tag{B.16}$$

thus defining $\mathbf{L}$. Correspondingly, we have

$$\tilde{\varepsilon}^{-1}_{\mathbf{G}\mathbf{0}}(\Omega_{\mathbf{k}}) = -\frac{\hat{\mathbf{k}}\cdot\mathbf{S}(\mathbf{G})}{\hat{\mathbf{k}}^{\mathrm{T}}\mathbf{L}\hat{\mathbf{k}}} , \tag{B.17}$$

$$\tilde{\varepsilon}^{-1}_{\mathbf{G}\mathbf{G}'}(\Omega_{\mathbf{k}}) = B^{-1}_{\mathbf{G}\mathbf{G}'} + \frac{\big[\hat{\mathbf{k}}\cdot\mathbf{S}(\mathbf{G})\big]\big[\hat{\mathbf{k}}\cdot\mathbf{S}^{*}(\mathbf{G}')\big]}{\hat{\mathbf{k}}^{\mathrm{T}}\mathbf{L}\hat{\mathbf{k}}} . \tag{B.18}$$

C Kleinman–Bylander correction to the matrix elements of the position operator

The matrix elements of $\mathbf{r}$, which enter the expressions in the previous section, are in practice calculated via the commutator of $\mathbf{r}$ with the Kohn–Sham Hamiltonian h^{KS} as

$$\langle\varphi_{c\mathbf{q}}|\mathbf{r}|\varphi_{v\mathbf{q}}\rangle = \frac{\langle\varphi_{c\mathbf{q}}|[h^{\mathrm{KS}},\mathbf{r}]|\varphi_{v\mathbf{q}}\rangle}{\epsilon_{c\mathbf{q}} - \epsilon_{v\mathbf{q}}} . \tag{C.1}$$

While the contribution from the kinetic-energy operator is trivial to compute, that from the non-local pseudopotential V_{nl} is more cumbersome and has often been neglected in earlier calculations. We show here that it is possible to compute it efficiently in a separable expression.

In its separable Kleinman–Bylander form [26] the non-local pseudopotential operator is written in the Dirac notation as

$$V_{\mathrm{nl}} = \sum_{\mu} |\phi_{\mu}\rangle \frac{1}{E_{\mu}} \langle\phi_{\mu}| , \tag{C.2}$$

where μ is a collective index $\{\mathbf{R}_\mu, n_\mu, l_\mu, m_\mu\}$ that runs over all pseudopotential projectors while ϕ_μ is in general given in a radial basis around a certain atomic position $\mathbf{R}_\mu$, i.e.,

$$\phi_\mu(\mathbf{r}) = f_{n_\mu l_\mu}(|\mathbf{r} - \mathbf{R}_\mu|) Y_{l_\mu m_\mu}(\Omega_{\mathbf{r}-\mathbf{R}_\mu}) \; . \tag{C.3}$$

In addition μ can run over chemical species, which does not alter the following derivation, except that f_{nl} then also depends on the species. We will now show that the commutator can be factorised, which reduces the scaling to be linear in the number of plane waves instead of quadratic as demonstrated in a previous approach [38]. To this end we consider the commutator of $\mathbf{r}$ with a single projector

$$\begin{aligned} &\Big(|\phi_\mu\rangle \frac{1}{E_\mu} \langle\phi_\mu|\mathbf{r}\Big) \; - \; \Big(\mathbf{r}|\phi_\mu\rangle \frac{1}{E_\mu} \langle\phi_\mu|\Big) \\ =& \frac{1}{E_\mu}\Big[|\phi_\mu\rangle\langle\phi_\mu|(\mathbf{r} - \mathbf{R}_\mu) \; - \; (\mathbf{r} - \mathbf{R}_\mu)|\phi_\mu\rangle\langle\phi_\mu|\Big] \; . \end{aligned} \tag{C.4}$$

Next we make use of the fact that $\mathbf{r} - \mathbf{R}_\mu$ can be expressed in the same radial basis as ϕ_μ

$$[\mathbf{r} - \mathbf{R}_\mu]_\alpha = |\mathbf{r} - \mathbf{R}_\mu| \sum_{m=-1}^{1} c_{\alpha m} Y_{1m}(\Omega_{\mathbf{r}-\mathbf{R}_\mu}) \; , \tag{C.5}$$

where $\alpha \in \{x, y, z\}$ are the spatial directions, and $c_{\alpha m}$ yield the spatial components of the spherical harmonics for $l = 1$:

$c_{\alpha m}$	$\alpha = x$	$\alpha = y$	$\alpha = z$
$m = -1$	$\frac{1}{\sqrt{2}}$	$\frac{i}{\sqrt{2}}$	0
$m = 0$	0	0	1
$m = 1$	$-\frac{1}{\sqrt{2}}$	$\frac{i}{\sqrt{2}}$	0

We can then write the product in the radial basis, too,

$$\begin{aligned} |\phi_\mu^\alpha\rangle :=& [\mathbf{r} - \mathbf{R}_\mu]_\alpha |\phi_\mu\rangle \\ =& |\mathbf{r} - \mathbf{R}_\mu| \sum_{m=-1}^{1} c_{\alpha m} Y_{1m}(\Omega_{\mathbf{r}-\mathbf{R}_\mu}) f_{n_\mu l_\mu}(|\mathbf{r} - \mathbf{R}_\mu|) Y_{l_\mu m_\mu}(\Omega_{\mathbf{r}-\mathbf{R}_\mu}) \\ =& \sum_{L=|l_\mu-1|}^{l_\mu+1} \sum_{M=-L}^{L} c_{\alpha M, m_\mu}^{L, l_\mu} f^{\mathrm{r}}_{n_\mu l_\mu}(|\mathbf{r} - \mathbf{R}_\mu|) Y_{LM}(\Omega_{\mathbf{r}-\mathbf{R}_\mu}) \end{aligned} \tag{C.6}$$

with

$$f^{\mathrm{r}}_{nl}(\rho) = \rho f_{nl}(\rho) \ , \tag{C.7}$$

$$c^{L,l}_{\alpha M,m} = \sum_{m'} c_{\alpha m'}(lm\ 1m'|LM) \ , \tag{C.8}$$

where $(lm\ 1m'|LM)$ is a Clebsch–Gordan coefficient. It is convenient to express ϕ^α_μ in a plane-wave basis similar to what is done for ϕ_μ. If the functions f_{nl} are given on a radial grid [39], f^{r}_{nl} is trivial to compute, and the same routines that are used to compute $\phi_\mu(\mathbf{k}+\mathbf{G})$ in the DFT calculation can be employed for the summands in $\phi^\alpha_\mu(\mathbf{k}+\mathbf{G})$. It must be emphasised that the sums over L and M contain only a very small number of non-zero terms (at most six).

The final formula is thus again a separable expression

$$[V_{\mathrm{nl}}, r_\alpha] = \sum_\mu \frac{1}{E_\mu} \left(|\phi_\mu\rangle\langle\phi^\alpha_\mu| - |\phi^\alpha_\mu\rangle\langle\phi_\mu| \right) \ . \tag{C.9}$$

The computational effort to set up a full $N_v \times N_c$ matrix for all three directions requires $4N_{\mathbf{G}}N_\mu(N_v+N_c)$ operations to calculate the $\langle\phi_\mu|\varphi_{v/c}\rangle$ and $\langle\phi^\alpha_\mu|\varphi_{v/c}\rangle$ projections and $6N_\mu N_v N_c$ operations to build up the 3 matrices from the projections in Equation (C.9). The scaling is thus linear in the number of $\mathbf{G}$-vectors $N_{\mathbf{G}}$ and not quadratic [38].

We have tested the size of the contributions from the non-local part of the pseudopotential for GaN and the II-VI compounds ZnO, ZnS, and CdS. We found that the macroscopic dielectric constant changes between +8 and –15%, which results in changes of the quasiparticle energies between –0.03 eV and 0.15 eV [3].

References

[1] L. Hedin, Phys. Rev. 139 (1965) A796.

[2] W. G. Aulbur, L. Jönsson, and J. W. Wilkins in Solid State Physics, edited by H. Ehrenreich and F. Spaepen (Academic, New York, 2000), vol. 54, p 1.

[3] P. Rinke, A. Qteish, J. Neugebauer, C. Freysoldt, M. Scheffler, New J. Phys. 7 (2005) 126.

[4] S. Biermann, F. Aryasetiawan, A. Georges, Phys. Rev. Lett. 90 (2003) 086402.

[5] P. Sun, G. Kotliar, Phys. Rev. Lett. 92 (2004) 196402.

[6] N. E. Zein, S. Y. Savrasov, G. Kotliar, Phys. Rev. Lett 96 (2006) 226403.

[7] G. Onida, L. Reining, A. Rubio, Rev. Mod. Phys. 74 (2002) 601.

[8] H. N. Rojas, R. W. Godby, R. J. Needs, Phys. Rev. Lett. 74 (1995) 1827.

[9] M. Rohlfing, P. Krüger, J. Pollmann, Phys. Rev. B 52 (1995) 1905.

[10] F. Aryasetiawan, O. Gunnarsson, Phys. Rev. Lett. 74 (1995) 3221, and references therein.

[11] S. Lebègue, B. Arnaud, M. Alouani, P. E. Bloechl, Phys. Rev. B 67 (2003) 155208.

[12] S. Galamić-Mulaomerović, C. H. Patterson, Phys. Rev. B 71 (2005) 195103.

[13] M. L. Tiago, J. R. Chelikowsky, Solid State Commun. 136 (2005) 333.

[14] M. L. Tiago, J. R. Chelikowsky, Phys. Rev. B 73 (2006) 205334.

[15] M. S. Hybertsen, S. G. Louie, Phys. Rev. B 34 (1986) 5390.

[16] Z. H. Levine, S. G. Louie, Phys. Rev. B 25 (1982) 6310.

[17] M. S. Hybertsen, S. G. Louie, Phys. Rev. B 37 (1988) 2733.

[18] G. Cappellini, R. Del Sole, L. Reining, F. Bechstedt, Phys. Rev. B 47 (1993) 9892.

[19] M. Palummo, R. Del Sole, L. Reining, F. Bechstedt, G. Cappellini, Solid State Commun. 95 (1995) 393.

[20] M. M. Rieger, L. Steinbeck, I. D. White, H. N. Rojas, R. W. Godby, Comput. Phys. Commun. 117 (1999) 211.

[21] R. Hott, Phys. Rev. B 44 (1991) 1057.

[22] O. Pulci, G. Onida, R. Del Sole, Phys. Rev. Lett. 81 (1998) 5374.

[23] B. Wenzien, G. Cappellini, F. Bechstedt, Phys. Rev. B 51 (1994) 14701.

[24] G. Fratesi, G. P. Brivio, P. Rinke, R. W. Godby, Phys. Rev. B 68 (2003) 195404.

[25] G. Fratesi, G. P. Brivio, L. G. Molinari, Phys. Rev. B 69 (2004) 245113.

[26] L. Kleinman, D. M. Bylander, Phys. Rev. Lett. 48 (1982) 1425.

[27] L. Steinbeck, A. Rubio, L. Reining, M. Torrent, I. D. White, R. W. Godby, Comput. Phys. Commun. 125 (2000) 105.

[28] R. M. Pick, M. H. Cohen, R. M. Martin, Phys. Rev. B 1 (1970) 910.

[29] J. D. Jackson, Classical electrodynamics, Wiley, 1975, p. 767.

[30] M. Abramowitz, I. A. Stegun (Eds.), Handbook of mathematical functions, Dover Publications, 1972, p. 1006.

[31] J. C. Phillips, L. Kleinman, Phys. Rev. 128 (1962) 2098.

[32] R. W. Godby, M. Schlüter, L. J. Sham, Phys. Rev. B 37 (1988) 10159.

[33] P. Eggert, Theoretische Untersuchung von Vielteilcheneffekten auf Silizium-Halbleiteroberflächen, Ph.D. thesis, Freie Universität Berlin (2005).

[34] V. I. Lebedev, D. N. Laikov, Doklady Mathematics 59 (1999) 477, fortran code is distributed through CCL (http://www.ccl.net/).

[35] S. Baroni, R. Resta, Phys. Rev. B 33 (1986) 7017.

[36] S. L. Adler, Phys. Rev. 126 (1962) 413.

[37] N. Wiser, Phys. Rev. 129 (1963) 62.

[38] V. Olevano, M. Palummo, G. Onida, R. Del Sole, Phys. Rev. B 60 (1999) 14224.

[39] M. Fuchs, M. Scheffler, Comput. Phys. Commun. 119 (1999) 67.